Critical scaling and percolation in manganite films

2001 J. Phys.: Condens. Matter 13 2919

(http://iopscience.iop.org/0953-8984/13/13/306)

INSTITUTE OF PHYSICS PUBLISHING JOURNAL OF PHYSICS: CONDENSED MATTER

J. Phys.: Condens. Matter **13** (2001) 2919–2934 www.iop.org/Journals/cm PII: S0953-8984(01)17673-3

Critical scaling and percolation in manganite films

M Ziese

Department of Superconductivity and Magnetism, University of Leipzig, Linnéstrasse 5, 04103 Leipzig, Germany

Received 31 October 2000, in final form 25 January 2001

Abstract

In this work the critical behaviour of films of $La_{0.7}Ba_{0.3}MnO_3$, $La_{0.7}Sr_{0.3}MnO_3$, $La_{0.7}Ca_{0.3}MnO_3$ and $(LaMn)_{1-\delta}O_3$ is studied. Apart from the $La_{0.7}Ca_{0.3}MnO_3$ film, each of these manganite films shows a continuous phase transition with mean-field critical exponents. The analysis of the critical amplitudes indicates the formation of spin polarons. The zero-field resistivity of the $La_{0.7}Ca_{0.3}MnO_3$ film is consistent with a model of percolative phase separation.

1. Introduction

The perovskites $La_{0.7}A_{0.3}MnO_3$ with A = Ca, Sr, Ba, ..., show a ferromagnetic transition at a composition-dependent Curie temperature that is accompanied by a metal–semiconductor transition. The application of a magnetic field leads to a large shift of the transition temperature and a corresponding 'colossal' magnetoresistance (CMR). It is generally found that the magnitude of the magnetoresistance decreases with increasing Curie temperature; see [1]. The mechanisms underlying CMR are not fully understood. One basic ingredient is double exchange between Mn^{3+} and Mn^{4+} ions [2]. Furthermore, the electron–phonon interaction plays a decisive role as regards the localization of charge carriers [3] and the formation of spin polarons has been suggested [4]. There is experimental evidence for phase separation in some manganite compounds, especially at compositions close to charge ordering and with low Curie temperature [5–7]. Consequently, it has been proposed recently that phase separation and percolation are the driving mechanisms behind CMR; see [8, 9].

It is well known that the conductivity of the manganites is very sensitive to structural distortions [1]. Since the ferromagnetism in doped manganites arises through real charge transfer between the Mn sites and since the low-temperature mean free path does not exceed 1–2 lattice spacings [10], the exchange integral is likely to be of short range and the critical exponents might be close to those of the Heisenberg model. This was indeed found in a recent theoretical study [11].

In this work the transition region for manganite films with various compositions, namely $La_{0.7}Ba_{0.3}MnO_3$, $La_{0.7}Sr_{0.3}MnO_3$, $La_{0.7}Ca_{0.3}MnO_3$, $(LaMn)_{1-\delta}O_3$, has been studied by means of global magnetization and resistivity measurements. This investigation aims at the determination of the critical exponents, since the values reported in the literature show considerable scatter; see table 6. Moreover, an analysis of the critical amplitudes enables the determination of the fluctuating magnetic moment. It was found that $La_{0.7}Ba_{0.3}MnO_3$,

0953-8984/01/132919+16$30.00

$La_{0.7}Sr_{0.3}MnO_3$ and $(LaMn)_{1-\delta}O_3$ films exhibit a second-order phase transition with mean-field critical exponents. The fluctuating entities are spin polarons consisting of 2–3 Mn ions. The $La_{0.7}Ca_{0.3}MnO_3$ film does not show a continuous phase transition, but is more consistently described within a percolative phase-separation model.

2. Theoretical models and data analysis

2.1. Critical behaviour of the magnetization

In the vicinity of a second-order phase transition with Curie temperature T_C the existence of a diverging correlation length $\xi = \xi_0|1 - T/T_C|^{-\nu}$ leads to universal scaling laws for the saturation magnetization M_S and susceptibility χ. Using standard notation, these are given by [12]

$$M_S = M_0(1 - T/T_C)^{\beta} \tag{1}$$

$$\chi = \chi_0(T/T_C - 1)^{-\gamma} \tag{2}$$

defining the critical exponents β and γ. At the transition temperature the magnetization is related to the applied field H by

$$\mu_0 H = D(\mu_0 M_S)^{\delta} \tag{3}$$

which defines the critical exponent $\delta = 1 + \gamma/\beta$. μ_0 denotes the vacuum permeability. The critical exponents as well as the critical amplitudes M_0, $h_0 = \chi_0^{-1} M_0$ and D exhibit universal behaviour near the phase transition point. There are several universality classes with sets of critical indices that depend on the spin and spatial dimensionality. Values for the mean-field, Ising and Heisenberg models are given in table 1 for spin $S = 1/2$ [13,14]. Whereas the critical indices do not depend on the magnitude of the spin quantum number, the critical amplitudes generally do; in mean-field theory one finds

$$M_0/M_S(0) = \left\{10(S+1)^2/3\left[(S+1)^2 + S^2\right]\right\}^{1/2} \tag{4}$$

$$\mu_0\mu h_0/k_B T_C = \left\{30S^2/\left[(S+1)^2 + S^2\right]\right\}^{1/2} \tag{5}$$

$$D(\mu_0 M_0)^{\delta}/\mu_0 h_0 = 1. \tag{6}$$

μ denotes the magnetic moment of the fluctuating entity, $\mu = gS\mu_B$, with electronic g-factor $g \simeq 2$ and Bohr magneton $\mu_B = e\hbar/2m$.

Table 1. Critical exponents and reduced critical amplitudes for the generic models used for the description of magnetic critical phenomena. The values are taken from [13] and [14].

Exponent	Mean-field theory	Heisenberg model	Ising model
β	0.5	0.365	0.325
γ	1.0	1.387	1.240
δ	3.0	4.803	4.816
ν	0.5	0.705	0.630
η	0.0	0.034	0.032
Reduced critical amplitude	Mean-field theory, $S = 1/2$	Heisenberg model, fcc, $S = 1/2$	Ising model, fcc, $S = 1/2$
$M_0/M_S(0)$	1.73	1.69	1.49
$\mu_0\mu h_0/k_B T_C$	1.73	1.58	1.52
$D(\mu_0 M_0)^{\delta}/\mu_0 h_0$	1.0	1.55	1.88

The spin–spin correlation function in the critical region obeys a scaling equation given by [12]

$$\langle \vec{S}_0 \cdot \vec{S}_{\vec{r}} \rangle = \frac{G(r/\xi)}{r^{1+\eta}}. \tag{7}$$

Here $\vec{S}_{\vec{r}}$ denotes a spin at position $\vec{r}$, $G(x)$ is an unknown scaling function; η signifies the deviation from the Ornstein–Zernicke result ($\eta = 0$) and is usually small, $0.01 \lesssim \eta \lesssim 0.04$ [15]. From the relation between the spin–spin correlation function and the susceptibility $\chi \propto \sum_{\vec{r}} \langle \vec{S}_0 \cdot \vec{S}_{\vec{r}} \rangle$ follows the scaling equation [12, 15]

$$\gamma = (2 - \eta)\nu. \tag{8}$$

In the critical region the magnetization obeys the scaling relation

$$\mu_0 M = |\epsilon|^{\beta} F_{\pm} \left[\mu_0 H |\epsilon|^{-\beta-\gamma} \right]. \tag{9}$$

The exact functional form of the scaling function F_- (F_+) below (above) the transition is unknown; the asymptotic forms for small and large arguments x are

$$F_-(0) = M_0 \tag{10}$$

$$F_+(x) \underset{x\to 0}{\sim} \chi_0 x \tag{11}$$

$$F_{\pm}(x) \underset{x\to\infty}{\sim} (D^{-1}x)^{1/\delta}. \tag{12}$$

For the comparison of experimental data with the idealized theory, several points have to be taken into account [12]. The phase transition temperature can usually not be directly measured, but has to be self-consistently determined from the analysis of the magnetization. In order to avoid effects due to magnetic domain formation or crystalline anisotropy, the saturation magnetization and susceptibility are determined by extrapolation from the high-field regime assuming an equation of state of the form [16]

$$[\chi_0 H/M]^{1/\gamma} = [T/T_C - 1] + [M/M_0]^{1/\beta}. \tag{13}$$

Once values for $\chi = M/H$ and M_S have been established by the above extrapolation procedure, these are analysed by two methods, namely (a) direct fitting using the critical amplitudes, exponents and the Curie temperature as free parameters and (b) the method of Kouvel and Fisher. The latter is based on the equations

$$[\mathrm{d}\ln(M_S)/\mathrm{d}T]^{-1} = (T - T_C)/\beta \tag{14}$$

$$\left[\mathrm{d}\ln(\chi^{-1})/\mathrm{d}T\right]^{-1} = (T - T_C)/\gamma. \tag{15}$$

The parameter values determined by the two methods were in good agreement. The Curie temperatures obtained from the analysis of the magnetization and susceptibility agreed within the experimental uncertainty.

2.2. Percolation theory

It has been proposed that the metal–semiconductor transition in the manganites can be understood as percolation of phase-separated metallic and insulating regions. Here the phase separation is not of charge-segregation type, since the length scales involved are much too large to be compatible with the Coulomb interaction. The percolation problem encountered in the manganites is obviously of continuum type and might be described by 'swiss-cheese' models [17, 18]. This, however, involves an unknown distribution function and non-universal critical exponents, thereby excluding a strict comparison of data to theory. Therefore, this work will be restricted to lattice percolation.

Consider a simple cubic lattice; metallic or semiconducting bonds are placed on this lattice with probabilities p and $q = 1 - p$, respectively. If p exceeds some critical value, the percolation threshold p_c, an infinite metallic cluster forms and the resistivity of the network becomes metallic. The system undergoes a second-order phase transition in complete analogy to the ferromagnetic phase transition with a diverging cluster size $\xi_p = \xi_{p0}|1 - p/p_c|^{-\nu_p}$. The corresponding quantities are the probability P that a bond belongs to the infinite cluster and the average cluster size S, which follow the scaling laws

$$P = P_0(p/p_c - 1)^{\beta_p} \tag{16}$$

$$S = S_0(1 - p/p_c)^{-\gamma_p}. \tag{17}$$

Values for the critical exponents and the percolation threshold are listed in table 2.

Table 2. Percolation exponents and percolation thresholds for 2D and 3D systems.

Exponent	$d = 2$	Reference	$d = 3$	Reference
β_p	5/36	[19]	0.41	[19]
γ_p	43/18	[19]	1.80	[19]
ν_p	4/3	[19]	0.88	[19]
t	1.299	[20]	1.98	[21]
s	1.299	[20]	0.73	[22]
p_c (bond), simple cubic	0.5	[19]	0.2488	[19]
p_c (site), simple cubic	0.5	[19]	0.3116	[19]

The correlation function at the percolation threshold decays algebraically, $g(r) \propto r^{-(d-2+\eta_p)}$, with $(d - 2 + \eta_p)\nu_p = 2\beta_p$. d is the spatial dimension. An inspection of the values for β_p and ν_p in table 2 shows that η_p is small as in the case of ferromagnets.

More interesting in the present work are the conductivity exponents t and s which are defined as follows. Consider a metal–insulator network with metallic and insulating bonds placed on a regular lattice with probabilities p and $q = 1-p$, respectively. Near the percolation threshold the conductivity of the network vanishes as

$$\sigma \propto (p - p_c)^t \qquad p > p_c. \tag{18}$$

If one considers a metal–superconductor network with occupation probabilities p (metal) and $q = 1 - p$ (superconductor), the conductivity diverges as the percolation threshold is approached:

$$\sigma \propto (q_c - q)^{-s} \qquad q < q_c. \tag{19}$$

Values for the critical exponents found numerically are listed in table 2.

In general, the averaged conductivity Σ of a binary mixture with resistivities ρ_m (probability p) and ρ_s (probability $q = 1 - p$) can be written as $\Sigma = F_2(p, \rho_m, \rho_s)$ with F_2 being an unknown function. In the case of phase separation in the manganites, ρ_m and ρ_s denote the resistivities of the metallic and semiconducting fractions, respectively. Dimensional analysis implies that F_2 is a homogeneous function of the bond resistivities such that the conductivity can be written as $\Sigma = \rho_m^{-1} F_1(p, h)$ with $h = \rho_m/\rho_s$ and $F_1(p, h) = F_2(p, 1, h^{-1})$. In the limits $h = 0$ and $h = \infty$ this corresponds to the metal–insulator and metal–superconductor networks with the aforementioned critical behaviour near p_c and q_c, respectively. For a general binary mixture, however, h is finite. Near the critical point $p = p_c$, $h = 0$ the following scaling behaviour was found to apply [23]:

$$\Sigma = \rho_m^{-1}|\Delta p|^t \Phi_\pm \left[h|\Delta p|^{-s-t}\right] \tag{20}$$

with $\Delta p = p - p_c$ and the scaling function Φ_+ (Φ_-) above (below) the transition. These have the asymptotic forms

$$\Phi_+(x) \underset{x\to 0}{\sim} \Phi_0 \tag{21}$$

$$\Phi_-(x) \underset{x\to 0}{\sim} x/x_0 \tag{22}$$

$$\Phi_\pm(x) \underset{x\to \infty}{\sim} K x^{t/(s+t)}. \tag{23}$$

In order to describe the behaviour across the transition, it is often more convenient to define a new function

$$\Psi(y) = y^t \Phi_+(y^{-s-t}) = (-y)^t \Phi_-[(-y)^{-s-t}]$$

such that

$$\Sigma = \rho_m^{-1} h^{t/(s+t)} \Psi\left[\Delta p\, h^{-1/(s+t)}\right]. \tag{24}$$

The exact form of the scaling functions $\Phi_\pm$, Ψ is unknown. Ψ is analytic and can be expanded in powers of y, $\Psi(y) = \Psi_0 + \Psi_1 y + \cdots$. In two-dimensional systems, $\Psi_0 = 1$ by virtue of the duality symmetry. At the percolation transition, $y = 0$, and the average resistivity $\rho = 1/\Sigma$ is given by

$$\rho = (\rho_m^s \rho_s^t)^{1/(s+t)} \frac{1}{\Psi_0} \tag{25}$$

which can be used to determine p_c from resistivity data.

A good approximation to the resistivity of binary mixtures not too close to the percolation threshold can be obtained within the effective-medium approximation (EMA) (see [23] and references cited therein). The EMA is a self-consistent scheme for determining the effective conductivity of a random mixture. In this scheme a fictitious network is considered, where all bonds have an effective conductance Σ except for one particular bond that has a conductance chosen randomly from the conductance distribution. If an electric field is applied to the network along the direction of this particular bond, a potential V_σ develops over this bond, whereas a voltage V is measured over all bonds far from this perturbation. The EMA requires this voltage fluctuation to vanish if averaged over the conductivity distribution; from this self-consistency condition the effective conductivity of a binary random mixture is obtained as

$$\Sigma = \rho_m^{-1} \frac{(p - p_c) + (q - p_c)h + \sqrt{(p - p_c)^2 + (q - p_c)^2 h^2 + 2(p_c - p_c^2 + pq)h}}{2(1 - p_c)}. \tag{26}$$

with $p_c = 1/d$. If both Δp and h are small in modulus, an approximation to the scaling function $\Psi(y)$ can be derived from equation (26):

$$\Psi(y) = \frac{\left[d^2 y^2 + 4(d-1)\right]^{1/2} + dy}{2(d-1)}. \tag{27}$$

3. Film preparation and experimental details

$La_{0.7}A_{0.3}MnO_3$, A = Ca, Sr, Ba, and $(LaMn)_{1-\delta}O_3$ films were grown by pulsed laser ablation (XeCl, 308 nm) from stoichiometric targets at an oxygen partial pressure of 100 mTorr and a substrate temperature of about 700 °C. The LSMO target was bought commercially; it was fabricated by a spray pyrolysis process which gives a good dispersion of the mixed oxides; the other three targets were fabricated by a standard solid-state reaction process. After removal from the deposition chamber the films were transferred to a furnace and annealed for 4 h at

950 °C in flowing O_2. High-quality epitaxial films were produced by this route on LSAT(001) substrates (LSAT $\equiv (LaAlO_3)_{0.3}(Sr_2TaAlO_6)_{0.7}$) with Curie temperatures ranging from 270 K (LCMO) to 360 K (LSMO) and low residual resistivities between 50 and 100 $\mu\Omega$ cm. The film thickness was determined from the deposition time and has an estimated error of about 10%. Here four films were investigated, with the parameters listed in table 3.

Table 3. Parameters of the manganite films investigated in this work.

Composition	Thickness (nm)	Curie temperature (K)
$La_{0.7}Ca_{0.3}MnO_3$ (LCMO)	150	271.0 K
$La_{0.7}Sr_{0.3}MnO_3$ (LSMO)	130	360.6 K
$La_{0.7}Ba_{0.3}MnO_3$ (LBMO)	150	311.2 K
$(LaMn)_{1-\delta}O_3$ (LMO)	150	288.3 K

In this work we report extensive magnetization measurements in the critical region of the manganite films. The measurements were performed with a superconducting quantum interference device (SQUID) magnetometer (MPMS-7, Quantum Design) with the field applied parallel to the film surface along [100]. In this configuration, demagnetizing effects are negligible. The isothermal magnetization of the films was measured after warming above the Curie temperature. The temperature stability was about ± 0.01 K. The magnetization of the LSAT substrate was measured at six temperatures in the range between 250 and 370 K and was found to be diamagnetic with a very small ferromagnetic signal, probably due to impurities. This background magnetization was interpolated to the respective measurement temperatures and subtracted from the measured film magnetization. Resistivity measurements were performed with a standard dc four-point technique in van der Pauw geometry [24].

4. Results

The magnetizations of the four manganite films recorded in an applied field of 0.3 T are shown in figure 1. Each film shows a saturation magnetization $\mu_0 M_S$ at low temperatures of about 0.74 T in agreement with a mean magnetic moment of 3.7 μ_B/unit cell. From the inflection point of the magnetization, the Curie temperatures can be estimated to be: 271.1 K (LCMO), 288.4 K (LMO), 312.6 K (LBMO) and 360.8 K (LSMO). The transition width depends on the doping, with the LCMO films having the sharpest and the LBMO film having the most gradual transition. Since the LSMO target is thought to be of better quality than the home-made LCMO target, this variation in transition width is likely to reflect an intrinsic mechanism rather than compositional inhomogeneity.

4.1. $(LaMn)_{1-\delta}O_3$, $La_{0.7}Sr_{0.3}MnO_3$ and $La_{0.7}Ba_{0.3}MnO_3$

After the Curie temperature had been estimated from the inflection point in the magnetization, sets of magnetization isotherms were measured in the transition region with a temperature separation of $\Delta T = 1.5$ K. A set of isotherms is shown in figure 2 for the LSMO film for temperatures ranging from 345 to 378 K. One can see a gradual transition from clearly ferromagnetic behaviour at low temperatures to nearly paramagnetic behaviour at high temperatures.

For further analysis, the isothermal magnetization data were replotted according to the equation of state (13) with the critical exponents β and γ used as variable parameters. For the LMO, LSMO and LBMO films, sets of straight lines could be produced with the choice

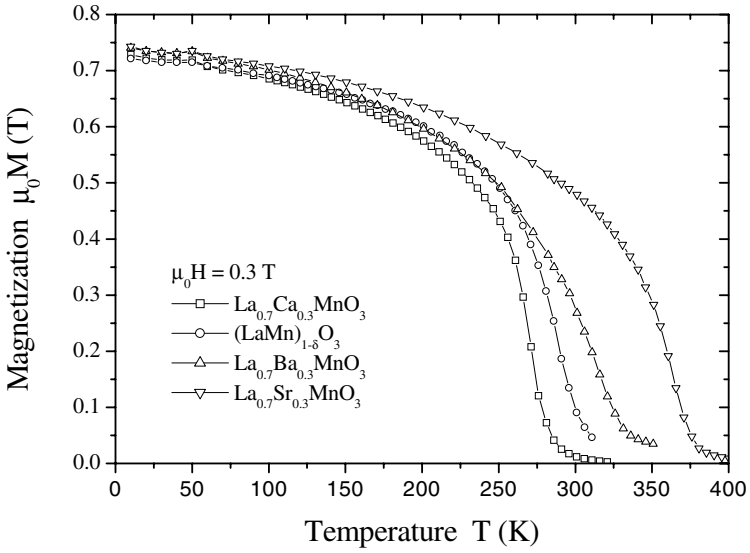

Figure 1. Magnetizations of the four manganite films investigated as functions of the temperature. The measurements were performed in an applied field of 0.3 T and the diamagnetic signal from the substrate was subtracted.

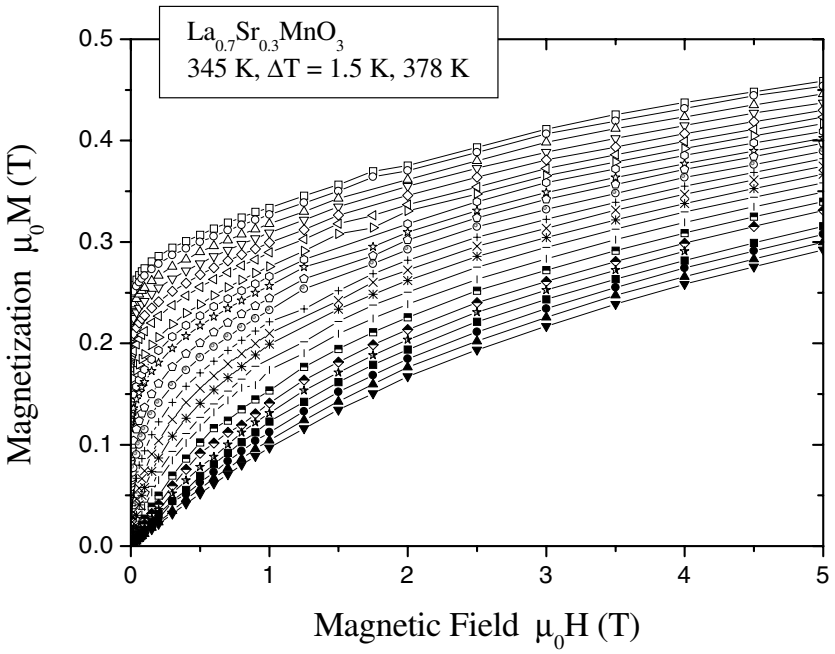

Figure 2. Magnetization isotherms recorded for the LSMO film in the critical region.

$\beta = 0.5 \pm 0.05$ and $\gamma = 1.0 \pm 0.05$; the LCMO film did not follow equation (13) for any reasonable choice of parameters; see below. Therefore, the critical behaviour of the LMO, LSMO and LBMO films will be discussed first. An Arrott plot for the LMO film is shown in figure 3.

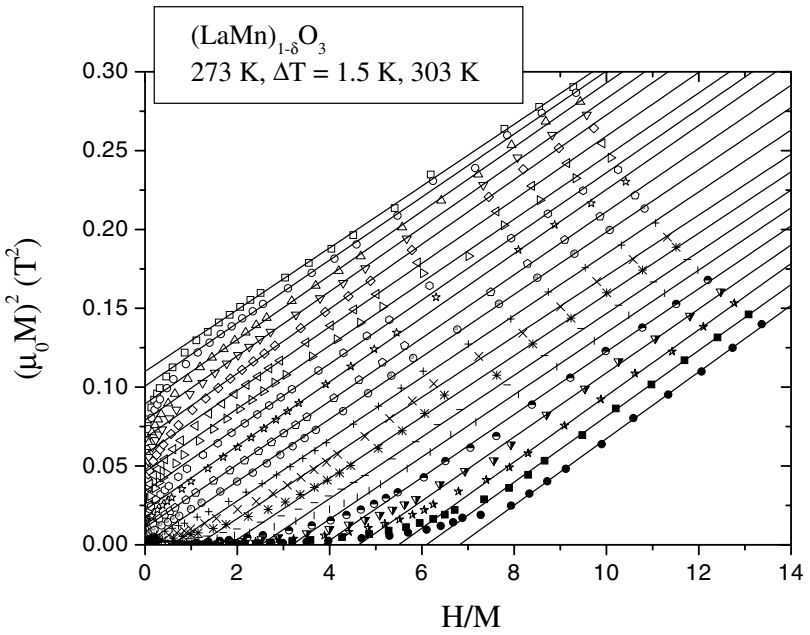

Figure 3. An Arrott plot for the LMO film showing a set of straight lines at high magnetic fields.

The values for the saturation magnetization M_S and susceptibility χ were determined by extrapolation of the high-field regime in the Arrott plot. The resulting data were analysed as discussed in section 2.1. The critical exponent δ was determined by fitting the magnetization isotherm closest to the Curie temperature to equation (3). The values for the Curie temperature, critical exponents and critical amplitudes are listed in table 4. The saturation magnetization and susceptibility are shown in figure 4 as a function of the reduced temperature.

Table 4. Curie temperatures, critical exponents and critical amplitudes determined from the analysis of the saturation magnetization and susceptibility.

Film	LSMO	LBMO	LMO
T_C (K)	360.0 ± 0.3	311.2 ± 0.2	288.3 ± 0.3
β	0.45 ± 0.02	0.54 ± 0.02	0.50 ± 0.01
γ	1.08 ± 0.04	1.04 ± 0.04	1.04 ± 0.04
δ	3.04 ± 0.04	3.08 ± 0.04	3.06 ± 0.03
$\mu_0 M_0$ (T)	1.18 ± 0.07	1.25 ± 0.04	1.48 ± 0.04
χ_0^{-1}	190 ± 20	137 ± 13	152 ± 14
D (T^{-2})	83.0 ± 2.0	96.0 ± 3.1	53.7 ± 0.3

The critical exponents found for the LMO, LSMO and LBMO films are quite close to the mean-field ones. Mean-field critical exponents were predicted to occur in systems with long-range exchange interactions of the form $J(r) \sim r^{-d-v}$ with $2v < d$; d is the spatial dimension [25]. It is quite surprising that manganite films show mean-field critical exponents, since the magnetic interaction is mediated by the double-exchange mechanism and is supposed to be short range: even at low temperatures, typical mean free paths do not exceed 1–2 lattice spacings [10]. An indication of the underlying mechanism comes from an inspection of the reduced critical amplitudes which are presented in table 5. The agreement of the experimentally

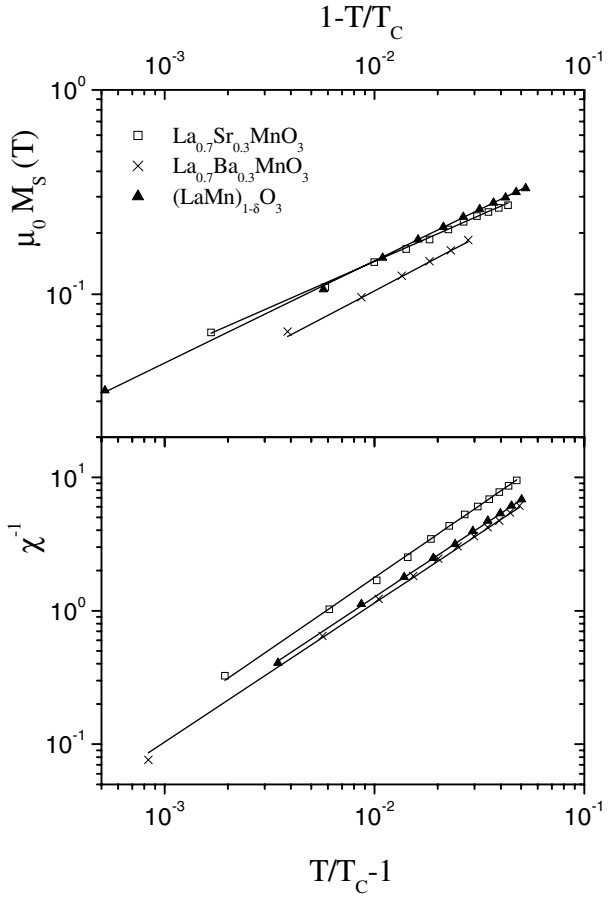

Figure 4. The saturation magnetization and susceptibility for the LMO, LSMO and LBMO films as functions of the reduced temperature.

Table 5. Reduced critical amplitudes. The magnetic moment μ was calculated using the values of the spin quantum number S given in the table.

Film	$M_0/M_S(0)$	$D(\mu_0 M_0)^\delta/k_B T_C$	S	$\mu_0\mu h_0/k_B T_C$	$\mu_0\mu h_0/k_B T_C\|_{\text{theoretical}}$
LSMO	1.59 ± 0.10	0.61 ± 0.10	3.7/2	1.55 ± 0.19	2.98
			7/2	2.92 ± 0.35	3.36
			11/2	4.59 ± 0.56	3.54
LBMO	1.69 ± 0.10	1.11 ± 0.13	3.7/2	1.39 ± 0.14	2.98
			7/2	2.59 ± 0.26	3.36
			11/2	4.07 ± 0.41	3.54
LMO	2.00 ± 0.10	0.79 ± 0.09	3.7/2	1.94 ± 0.19	2.98
			7/2	3.67 ± 0.35	3.36
			11/2	5.77 ± 0.55	3.54

determined reduced critical amplitudes $M_0/M_S(0)$ and $D(\mu_0 M_0)^\delta/(\mu_0 h_0)$ with the prediction of mean-field theory is satisfactory. This is encouraging, since the critical amplitudes are much more affected by corrections to scaling than the critical exponents. The measured reduced

amplitude $\mu_0\mu h_0/(k_B T_C)$, however, is found to be systematically smaller than the theoretical value, if a mean magnetic moment $\mu = 3.7\ \mu_B$ is assumed. This critical amplitude indicates that the moment of the fluctuating entity is larger than a single Mn-ion moment and is in the range between 7 and 11 μ_B corresponding to small clusters of two or three Mn ions. This is consistent with the results of pulsed neutron scattering studies on $La_{1-x}Sr_xMnO_3$ powder samples showing polarons extending over three Mn sites in the metallic phase [26] and with low-field magnetization measurements on polycrystalline $La_{0.67}Ca_{0.33}MnO_3$ samples [27].

The validity of the critical analysis was further checked by scaling of the magnetization isotherms following equation (9). The scaling plots are shown in figure 5 using the critical

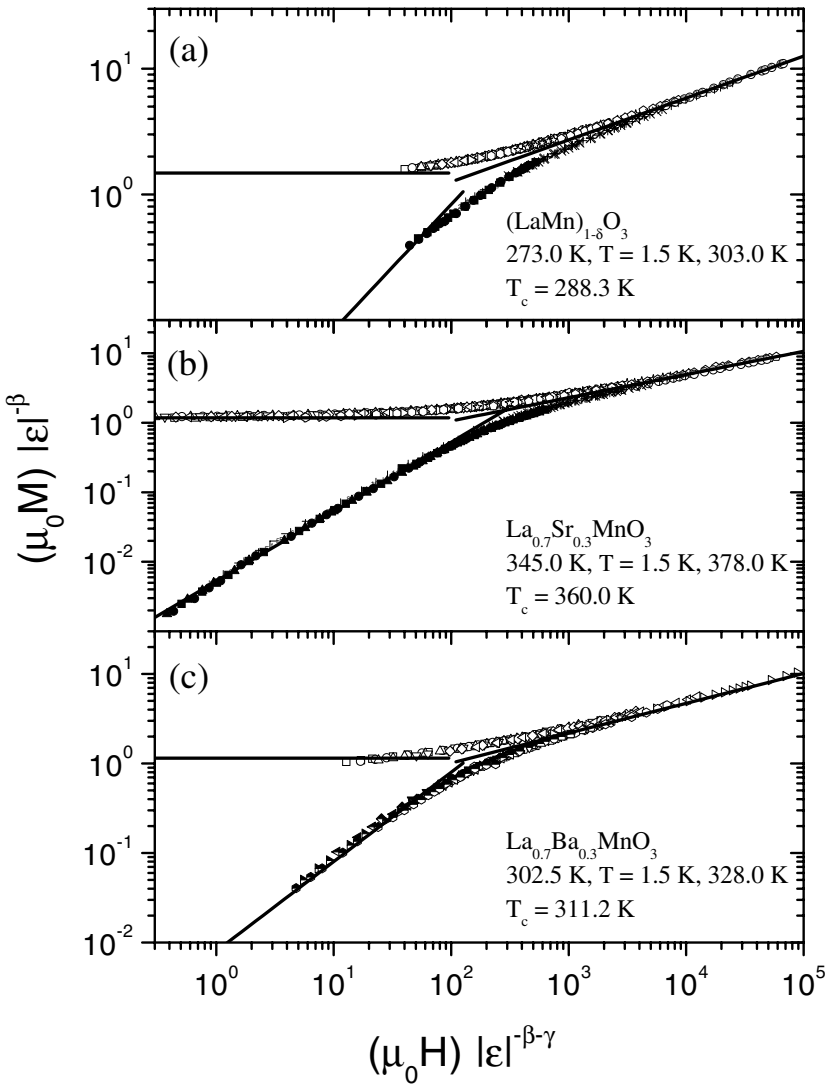

Figure 5. Scaling plots for the (a) $(LaMn)_{1-\delta}O_3$, (b) $La_{0.7}Sr_{0.3}MnO_3$ and (c) $La_{0.7}Ba_{0.3}MnO_3$ films showing a collapse of magnetization isotherms in the critical region onto the two branches of the scaling function. The solid lines indicate the asymptotic forms of the scaling function as given in equations (10)–(12).

exponents $\beta = 0.5$ and $\gamma = 1.0$. A convincing scaling of the data points on the two branches of the scaling function $F_{\pm}$ can be seen. The solid lines in figure 5 indicate the asymptotic forms of the scaling function as detailed in equations (10)–(12); the experimentally determined scaling function is in good agreement with these limiting forms.

4.2. $La_{0.7}Ca_{0.3}MnO_3$: percolation transition

In contrast to the data for LMO, LSMO and LBMO, the magnetization isotherms for LCMO did not follow the equation of state (13) for reasonable choices of the critical exponents $0.2 \leqslant \beta \leqslant 0.7$ and $0.8 \leqslant \gamma \leqslant 1.5$. An Arrott plot of the data is shown in figure 6 and confirms that the magnetization isotherms do not fall on straight lines. This finding is consistent with the results of Mira *et al* [28] and Moutis *et al* [29] on ceramic LCMO samples. These authors report negative slopes of the H/M versus M^2 plot which—according to a criterion given by Banerjee [30]—indicate a first-order transition. This crossover from a second-order to a first-order transition is consistent with the measured transition width. Although the Arrott plot of the LCMO film studied in this work does not show negative slopes, the transition might be close to first order, such that a critical scaling analysis fails in the field range investigated, $0 \leqslant \mu_0 H \leqslant 5$ T.

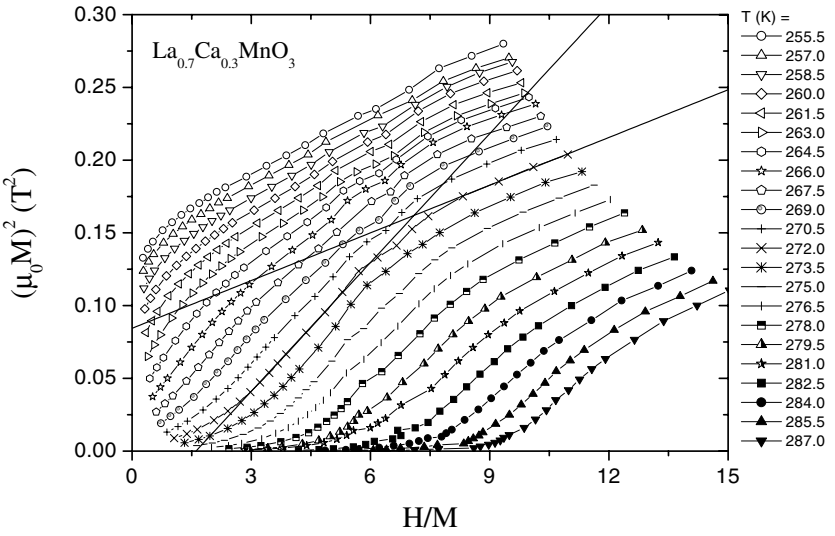

Figure 6. An Arrott plot for the $La_{0.7}Ca_{0.3}MnO_3$ film showing curvature of the magnetization isotherms over the whole measurement field range. The straight lines to the 272.0 K isotherm are used to perform a critical scaling analysis in the regime of intermediate and high field.

It is possible to perform critical scaling analyses in a regime of intermediate and high field; this is indicated by the straight lines to the 272.0 K isotherm. However, such an analysis is *a priori* doubtful, since a continuous phase transition should be described by a unique transition temperature valid for a range of magnetic fields. Notwithstanding these doubts, the analysis of modified Arrott plots indicates critical exponents $\beta \sim 0.3$, $\gamma \sim 1.0$ and Curie temperatures $T_C \sim 270$ K (intermediate fields) and $T_C \sim 278$ K (high fields). The analysis, however, is not consistent, since the critical exponents obtained from the temperature dependence of M_S and χ are lower than the exponents used in the equation of state (13) even after some iterations. The data presented here do not support the scenario suggested by Xue *et al* [31] wherein the

critical regime in $La_{0.7}Pb_{0.3}MnO_3$ is dominated by mean-field fluctuations at low fields <1 T and by the Heisenberg model at large fields >1 T.

The observation that the order of the phase transition changes on decrease of T_C in the manganites is consistent with numerous reports of percolative phase transitions in low-T_C manganite phases [5,7,32,33]. On theoretical grounds it is expected that manganites showing phase separation have first-order transitions that might be driven towards second order by crystallographic disorder [9]. In order to investigate this mechanism in the case of the LCMO film, the resistivity transition is analysed within a model of percolative transport between a semiconducting and a metallic phase. The analysis of the magnetization data indicated $\gamma \sim 1$ and—in view of the mean-field behaviour of the manganite compounds with higher Curie temperature—it is reasonable to assume a mean-field model for LCMO. Thus $\eta = 0$ and the correlation length diverges with an exponent $\nu = 1/2$. Percolation theory is formulated in terms of the concentration p of the metallic phase which is a function of temperature. In the critical regime, the behaviour of the system is determined by the correlation length. Since there is overwhelming evidence that the transport and magnetic behaviour of the manganites are intimately linked, the magnetic correlation length and the percolation correlation length have to be equal:

$$\xi = \xi_0 |1 - T/T_C|^{-\nu} = \xi_{p0} |1 - p/p_c|^{-\nu_p} = \xi_p. \tag{28}$$

This equation determines a unique relation between concentration p and temperature.

In order to compare percolation theory and experimental data, the temperature dependence of the resistivity in the metallic and semiconducting phases has to be determined. This is performed outside the transition regime. In the ferromagnetic phase the resistivity is due to scattering by static disorder and first- and second-order magnon processes with [34]

$$\rho_m = \rho_0 + \rho_2 T^2 + \rho_{4.5} T^{4.5}. \tag{29}$$

In the semiconducting phase, charge transport occurs by hopping of small polarons [10]; thus

$$\rho_s = AT \exp[U/k_B T]. \tag{30}$$

Fitting of equations (29), (30) to the data yields the parameters $\rho_0 = 0.099$ mΩ cm, $\rho_2 = 6.9 \times 10^{-6}$ mΩ cm K^{-2} and $\rho_{4.5} = 6.7 \times 10^{-12}$ mΩ cm K$^{-4.5}$ in the ferromagnetic regime as well as $A = 1.4 \times 10^{-3}$ mΩ cm K^{-1} and $U = 65$ meV in the semiconducting phase. These asymptotic forms for the resistivity are shown in figure 7.

The resistivity in the transition regime was calculated within the effective-medium approximation, equation (26), using equations (28)–(30) as input. Since the films are rather thick, three-dimensional percolation is assumed. The critical temperature was determined from the inflection point of the magnetization to be $T_C = 271$ K. With only one free parameter—$\xi_0/\xi_{p0} = 0.8$—a convincing fit to the data could be obtained. The ratio of the critical amplitudes ξ_0 and ξ_{p0} is close to unity as expected. Note that the calculated curve reproduces the steep slope just at the metal–semiconductor transition quite well. This is due to the strong temperature dependence of the metallic fraction p near the percolation threshold, $|p - p_c| \propto |T - T_C|^{\nu/\nu_p}$ with $\nu/\nu_p = 0.57$ for a three-dimensional system showing mean-field behaviour. The resistivity calculated within the percolation model yielded a fit to the data for the LBMO film that was much worse than that for LCMO. This is consistent with the finding that the metal–semiconductor transition in LBMO is not of the percolation type, but is a homogeneous spin-polaron transition.

5. Discussion and conclusions

In this work the critical regime for various manganite films was investigated by the analysis of magnetization isotherms in the critical regime as well as the zero-field resistivity. It was

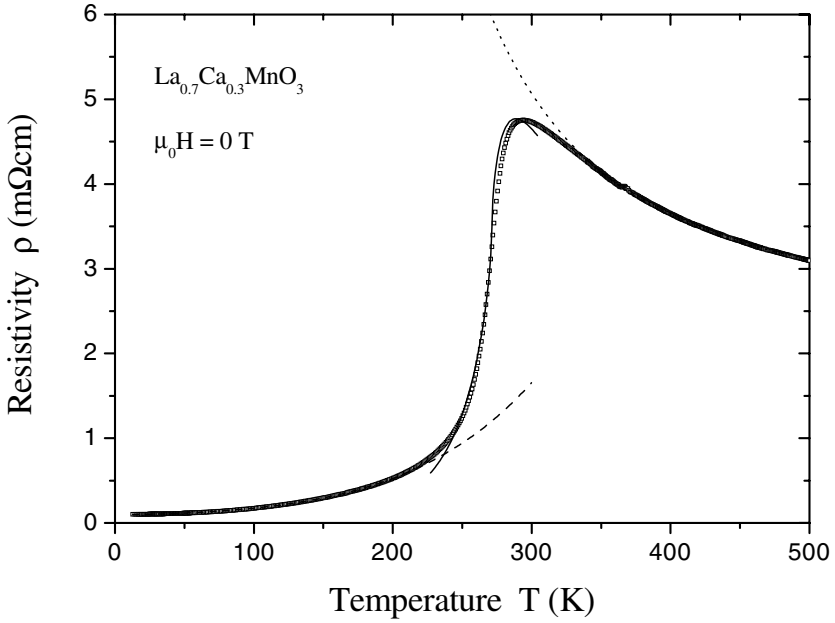

Figure 7. The zero-field resistivity of the LCMO film as a function of temperature. The dotted lines indicate the asymptotic forms of the resistivity in the metallic and semiconducting regimes. The solid line was calculated on the assumption of a percolation transition and using the effective-medium approximation.

found that films with composition $La_{0.7}Ba_{0.3}MnO_3$, $La_{0.7}Sr_{0.3}MnO_3$ and $(LaMn)_{1-\delta}O_3$ do show a second-order phase transition, whereas $La_{0.7}Ca_{0.3}MnO_3$ does not show a continuous transition. This finding is especially important for the theoretical description of the manganites, since it shows that despite all the similarities there might be different mechanisms underlying CMR depending on the exact composition of the material. The results of this work and the studies [5–7] show that the Curie temperature might be an indicator that can be used to classify the nature of the transition. Roughly speaking, manganite samples with Curie temperatures below ∼280 K do not show continuous phase transitions, whereas samples with higher Curie temperature clearly exhibit second-order phase transitions. Since phase separation was found in low-T_C samples, it is tempting to conclude that the ground state is inhomogeneous for these samples, whereas samples with high Curie temperature are homogeneous with the possible formation of spin polarons consisting of 2–3 Mn ions.

In the case of $La_{0.7}Ba_{0.3}MnO_3$, $La_{0.7}Sr_{0.3}MnO_3$ and $(LaMn)_{1-\delta}O_3$ the critical exponents found in this work are consistent with mean-field theory. This is in contrast with the findings of a recent investigation of the double-exchange mechanism using Monte Carlo simulations, which indicates critical exponents consistent with the Heisenberg model [11]. It was shown by Fisher *et al* [25] that the critical exponents approach the values of the Heisenberg model if the exchange interaction is decaying as $J(r) \sim r^{-d-v}$ with $2v > d$, whereas mean-field values are found for $2v < d$. Since the double-exchange mechanism is supposed to be of short range, critical behaviour consistent with the Heisenberg model might be expected. The reduced critical amplitudes indicate spin-polaron formation with a cluster size of about 2–3 Mn ions. This is consistent with calculations of the binding energy of Mn clusters performed by Gehring and Coombes [35]. These authors found that a Mn-ion triple containing one hole, i.e. a Mn^{3+}–Mn^{4+}–Mn^{3+} cluster, has a significant binding energy of about half the binding

energy of the bulk. These large spin moments enhance the dipole–dipole interaction; in the case of the Heisenberg model, however, corrections to the critical exponents due to the dipole–dipole interaction are rather small [36] and do not explain the observed mean-field values. The situation is different for the Ising model. In this case the critical dimensionality becomes $d = 3$, if dipole–dipole interactions are present; accordingly the correlation length and susceptibility diverge with mean-field exponents and logarithmic corrections, $\xi \propto |\epsilon|^{-1/2}|\ln(|\epsilon|)|^{1/6}$ and $\chi \propto |\epsilon|^{-1}$ for $|\epsilon| < G^{1/\phi}$ [37]. $G = \mu_0[(g\mu_B)^2 S(S+1)]/JS(S+1)a^3$ measures the relative strength of the dipole–dipole and exchange interactions; the crossover exponent is given by $\phi \simeq 7/6$. With $S = 11/2$, $JS(S+1) = k_B T_C/2$, $T_C \sim 300$ K and a lattice constant $a = 3.8$ Å, one obtains $|\epsilon| < 0.19$ which is obeyed in the experiments performed here. This discussion shows that the critical behaviour of manganite films is consistent with mean-field theory as well as with the Ising model including dipole–dipole interactions. It might be possible that the tetragonal distortion of the films leads to a change from Heisenberg to Ising behaviour.

Critical exponents and Curie temperatures determined for various manganite systems are listed in table 6. These values scatter in the ranges $\beta \sim 0.3$–0.5 and $\gamma \sim 1.0$–1.3. Schwartz *et al* [40] already criticized some of the values determined by means of μSR and neutron scattering, since the temperature range used for fitting was very wide with the analysis being performed in a relative temperature interval $\Delta T/T < 0.3$. The critical analysis reported here was performed in a temperature range $0.001 < T < 0.05$ and is expected to be more reliable. Furthermore, the microwave, μSR and neutron scattering techniques enable only the determination of the saturation magnetization; using bulk magnetization measurements, some cross-checks can be performed that yield more reliable data. For example, it is perfectly

Table 6. Critical exponents for manganite films as determined by various methods. $M(H)$ indicates bulk magnetization measurements, FMR denotes ferromagnetic resonance, FMAR ferromagnetic antiresonance, n-scattering stands for neutron scattering and μSR denotes μ^+ spin resonance.

Compound	Method	T_C (K)	β	γ	Reference
$La_{0.8}Sr_{0.2}MnO_3$	$M(H)$	315.7	0.50 ± 0.02	1.08 ± 0.03	[38]
$La_{0.7}Sr_{0.3}MnO_3$	$M(H)$	354.0	0.37 ± 0.04	1.22 ± 0.03	[39]
$La_{0.67}(Ba_xCa_{1-x})_{0.33}MnO_3$	$M(H)$				[29]
$x = 0.25$		276.7	0.36	1.12	
$x = 0.5$		306.1	0.40	1.11	
$x = 1.0$		338.1	0.46	1.29	
$La_{0.7}Pb_{0.3}MnO_3$	$M(H)$				[31]
	$\mu_0 H > 1$ T	334.4	0.33 ± 0.01	1.27 ± 0.02	
	$\mu_0 H < 1$ T	336.5	0.50 ± 0.02	1.0 ± 0.1	
$La_{0.7}Sr_{0.3}MnO_3$	$M(H)$	360.6	0.45 ± 0.02	1.08 ± 0.04	This work
$La_{0.7}Ba_{0.3}MnO_3$	$M(H)$	311.2	0.54 ± 0.02	1.04 ± 0.04	This work
$(LaMn)_{1-\delta}O_3$	$M(H)$	288.3	0.50 ± 0.01	1.04 ± 0.04	This work
$La_{0.7}Ca_{0.3}MnO_3$	$M(H)$	~ 271	—	—	This work
$La_{0.8}Sr_{0.2}MnO_3$	FMAR	305.5	0.45 ± 0.05	—	[40]
$La_{0.7}Sr_{0.3}MnO_3$	FMAR	361	0.45 ± 0.05	—	[41]
$La_{0.8}Sr_{0.2}MnO_3$	$M(H)$, FMR, FMAR	304	0.34 ± 0.05	—	[42]
$La_{0.7}Sr_{0.3}MnO_3$	n-scattering	378.1	0.295 ± 0.002	—	[43]
$La_{0.8}Sr_{0.2}MnO_3$	n-scattering	305.1	0.29 ± 0.01	—	[44]
$La_{0.7}Sr_{0.3}MnO_3$	n-scattering	350.8	0.30 ± 0.02	—	[44]
$La_{0.67}Ca_{0.33}MnO_3$	μSR	274.3	0.345 ± 0.015	—	[45]

possible to determine the saturation magnetization of the LCMO film studied in this work using a modified Arrott plot; however, fitting of $M_S(T)$ yields values for β that are inconsistent with the values used in the equation of state (13) and for extrapolation, thus indicating the breakdown of scaling. The direct measurement of the correlation length in a $La_{0.75}Sr_{0.25}MnO_3$ single crystal by means of small-angle neutron scattering yielded a critical exponent $\nu = 0.4$ rather close to the mean-field value [46]. One possibility for explaining the scatter in the critical exponents might be a dependence of spin-polaron formation on the microstructure with a resulting sample dependence of the critical exponents.

The resistivity of the LCMO film was analysed within a percolation model. Although this is not the first analysis of this kind—see [47–49]—here the exact scaling behaviour of the percolation transition was taken into account with only one free parameter, whereas previous studies determined the temperature-dependent metallic fraction p phenomenologically with a large set of fitting parameters. The fit of the percolation model used here to the data is quite satisfactory and shows that a description of this low-T_C manganite sample in terms of the percolation of phase-separated clusters is reasonable. Further studies are clearly necessary in order to understand the influence of an applied magnetic field on the transition.

Acknowledgments

The manganite films were fabricated at the University of Sheffield; that part of the work was supported by the European Union TMR 'OXSEN' network. I thank Professor G Gehring, University of Sheffield, for a critical reading of the manuscript. The work in Leipzig was supported by the Deutsche Forschungsgemeinschaft under DFG IK 24/B1-1 (project H).

References

[1] Coey J M D, Viret M and von Molnár S 1999 *Adv. Phys.* **48** 167
[2] Zener C 1951 *Phys. Rev.* **82** 403
[3] Millis A J, Shraiman B I and Mueller R 1996 *Phys. Rev. Lett.* **77** 175
[4] Röder H, Zang J and Bishop A R 1996 *Phys. Rev. Lett.* **76** 1356
[5] Uehara M, Mori S, Chen C H and Cheong S-W 1999 *Nature* **399** 560
[6] Fiebig M, Miyano K, Tomioka Y and Tokura Y 1998 *Science* **280** 1925
[7] Fäth M, Freisem S, Menovsky A A, Tomioka Y, Aarts J and Mydosh J A 1999 *Science* **285** 1540
[8] Moreo A, Yunoki S and Dagotto E 1999 *Science* **283** 2034
[9] Moreo A, Mayr M, Feiguin A, Yunoki S and Dagotto E 2000 *Phys. Rev. Lett.* **84** 5568
[10] Ziese M and Srinitiwarawong C 1998 *Phys. Rev.* B **58** 11 519
[11] Alonso J L, Fernández L A, Guinea F, Laliena V and Martín-Mayor V 2000 *Preprint* cond-mat/0007450
[12] Kadanoff L P, Götze W, Hamblen D, Hecht R, Lewis E A S, Palciauskas V V, Rayl M, Swift J, Aspnes D and Kane J 1967 *Rev. Mod. Phys.* **39** 395
[13] Le Guillou J C and Zinn-Justin J 1977 *Phys. Rev. Lett.* **39** 95
[14] Seeger M, Kronmüller H and Blythe H J 1995 *J. Magn. Magn. Mater.* **139** 312
[15] Fisher M E 1974 *Rev. Mod. Phys.* **46** 597
[16] Arrott A and Noakes J E 1967 *Phys. Rev. Lett.* **14** 786
[17] Feng S, Halperin B I and Sen P N 1987 *Phys. Rev.* B **35** 197
[18] Balberg I 1998 *Phys. Rev.* B **57** 13 351
[19] Stauffer D and Aharony A 1995 *Perkolationstheorie* (Weinheim: VCH)
[20] Normand J-M, Hajjar H J and Herrmann H J 1988 *J. Stat. Phys.* **52** 441
[21] Normand J-M and Herrmann H J 1995 *Int. J. Mod. Phys.* C **6** 813
[22] Normand J-M and Herrmann H J 1990 *Int. J. Mod. Phys.* C **1** 207
[23] Clerc J P, Giraud G, Laugier J M and Luck J M 1990 *Adv. Phys.* **39** 191
[24] van der Pauw L J 1958 *Philips Tech. Rev.* **20** 220
[25] Fisher M E, Ma S-K and Nickel B G 1972 *Phys. Rev. Lett.* **29** 917
[26] Louca D and Egami T 1999 *Phys. Rev.* B **59** 6193

[27] Amaral V S, Araújo J P, Pogorelov Yu G, Sousa J B, Tavares P B, Vieira J M, Lopes dos Santos J M B, Lourenço A A C S and Algarabel P A 1998 *J. Appl. Phys.* **83** 7154
[28] Mira J, Rivas J, Rivadulla F, Vázquez-Vázquez C and López-Quintela M A 1999 *Phys. Rev.* B **60** 2998
[29] Moutis N, Panagiotopoulos I, Pissas M and Niarchos D 1999 *Phys. Rev.* B **59** 1129
[30] Banerjee S K 1964 *Phys. Lett.* **12** 16
[31] Xue Y Y, Lorenz B, Heilman A K, Gospodinov M, Dobreva S G and Chu C W 2000 *Preprint* cond-mat/0002468
[32] Raquet B, Anane A, Wirth S, Xiong P and von Molnár S 2000 *Phys. Rev. Lett.* **84** 4485
[33] Merithew R D, Weissman M B, Hess F M, Spradling P, Nowak E R, O'Donnell J, Eckstein J N, Tokura Y and Tomioka Y 2000 *Phys. Rev. Lett.* **84** 3442
[34] Ziese M 2000 *Phys. Rev.* B **62** 1044
[35] Gehring G A and Coombes D J 1998 *J. Magn. Magn. Mater.* **177–181** 873
[36] Fisher M E and Aharony A 1973 *Phys. Rev. Lett.* **30** 559
Aharony A and Fisher M E 1973 *Phys. Rev.* B **8** 3323
[37] Aharony A 1973 *Phys. Rev.* B **8** 3363
[38] Mohan Ch V, Seeger M, Kronmüller H, Murugaraj P and Maier J 1998 *J. Magn. Magn. Mater.* **183** 348
[39] Ghosh K, Lobb C J, Greene R L, Karabashev S G, Shulyatev D A, Arsenov A A and Mokovskii Y 1998 *Phys. Rev. Lett.* **81** 4740
[40] Schwartz A, Scheffler M and Anlage S M 2000 *Phys. Rev.* B **61** R870
[41] Lofland S E, Ray V, Kim P H, Bhagat S M, Manheimer M A and Tyagi S D 1997 *Phys. Rev.* B **55** 2749
[42] Lofland S E, Bhagat S M, Ghosh K, Greene R L, Karabashev S G, Shulyatev D A, Arsenov A A and Mikovskii Y 1997 *Phys. Rev.* B **56** 13 705
[43] Martin M C, Shirane G, Endoh Y, Hirota K, Moritomo Y and Tokura Y 1996 *Phys. Rev.* B **53** 14 285
[44] Vasiliu-Doloc L, Lynn J W, Mukovskii Y M, Arsenov A A and Shulyatev D A 1998 *J. Appl. Phys.* **83** 7342
[45] Heffner R H, Le L P, Hundley M F, Neumeier J J, Luke G M, Kojima K, Nachumi B, Uemura Y J, MacLaughlin D E and Cheong S-W 1996 *Phys. Rev. Lett.* **77** 1869
[46] Viret M, Glättli H, Fermon C, De Leon-Guevara A M and Revcolevschi A 1998 *Europhys. Lett.* **42** 301
[47] Jaime M, Lin P, Chun S H, Salamon M B, Dorsey P and Rubinstein M 1999 *Phys. Rev.* B **60** 1028
[48] Song H, Kim W J and Kwon S-J 2000 *J. Magn. Magn. Mater.* **213** 126
[49] Mayr M, Moreo A, Vergés J A, Arispe J, Feiguin A and Dagotto E 2000 *Preprint* cond-mat/0007480